A report to the sponsors of the
Exploration Geophysics Laboratory

# Extraction and Imaging of SV-P Reflections from Far-Offset VSP Data

Yandong Li and Bob Hardage

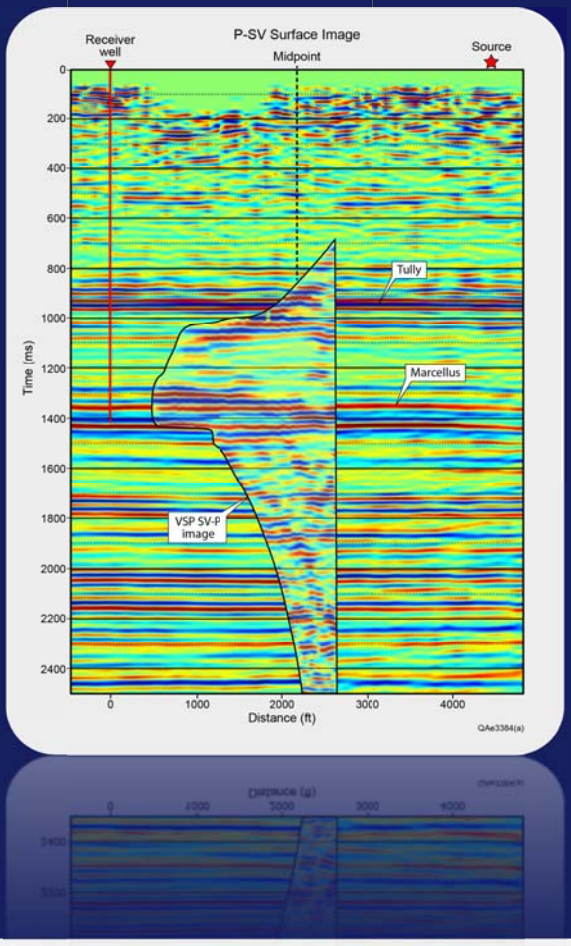


January 2015

EGL Exploration Geophysics Laboratory

Bureau of Economic Geology

QAe3388

The information in this EGL Sponsor Report will be submitted for publication in the SEG/AAPG journal **Interpretation**. Publication should occur in late 2015 or early 2016.

# Contents

## Abstract

We show in this report to sponsors of the Exploration Geophysics Laboratory (EGL) that SV-P reflections can be extracted from far-offset VSP data generated by a vertical-vibrator source using time-variant receiver rotations. Optimal receiver rotation angles are determined by a dynamic steering of geophones to the time-varying approach directions of upgoing SV-P reflections. These SV-P reflections are then imaged using a VSPCDP transformation based on ray-tracing. Comparisons of our SV-P image with P-P and P-SV images derived from the same offset VSP data show that for deep targets, SV-P data create an image that extends farther from the receiver well than P-P and P-SV images and that spans a wider offset range than P-P and P-SV images do. We compare our VSP SV-P image with a surface-based P-SV profile that traversed the VSP well. This comparison demonstrates that SV-P data are equivalent to P-SV data for characterizing geology. VSP derived SV-P images will be needed for calibrating surface-recorded SV-P data that are generated by the direct-S technology the Exploration Geophysics Laboratory is developing.

## Introduction

Hardage et al. (2014) proposed that SV-P data, although being ignored by the seismic-user community, are seismic modes that have great value for interpreters. In any comparative metric one uses, SV-P images should be as informative and as valuable as P-SV images for seismic interpretation purposes. Some of the advantages of surface-based SV-P technology are:

(1) The seismic sources needed to generate SV-P data are common P-wave sources that are widely spread around the globe;

(2) SV-P data are recorded by vertical geophones. In contrast, P-SV data must be recorded by horizontal geophones, which requires that 3C geophones be deployed. There is a cost savings in data acquisition when vertical geophones are used rather than 3C geophones.

(3) Because a P-wave source generates an SV illuminating wavefield directly at the source station and the upgoing converted-P mode is recorded by vertical geophones, there is a huge amount of untapped SV-P data in legacy P-wave seismic data (Hardage and Wagner, 2014). Interpreters may be able to produce valuable S-wave images from these legacy P-wave data without paying the cost of new S-wave data recording. Therefore, SV-P data can be the lowest cost and most widely available source of S-wave information for the global seismic interpretation community (Hardage et al., 2014).

The geophysical literature that discusses real SV-P data is quite limited. We can find only four papers that show real SV-P data (Fraiser and Winterstein, 1990; Guy, 2004; Hardage et al. 2014; DeAngelo and Hardage, 2014). Fraiser and Winsterstein (1990) investigated SV-P reflections along a single 2D line of 9-component seismic data. Guy (2004) acquired a short SV-P profile approximately 300 ft long and studied shallow strata extending to a depth of approximately 70 ft. Both of these investigations focused on SV-P data generated by a horizontal vibrator and made no SV-P images from P-wave source data. In contrast, DeAngelo and Hardage (2014) compared P-P, P-SV, and SV-P surface-based images produced by an array of vertical vibrators. However, none of these studies had VSP derived SV-P images for calibrating their surface-recorded SV-P data. Hardage et al. (2014) showed that upgoing SV-P reflections could be extracted from far-offset VSP data using a fixed-angle additional-rotation approach. However, they did not produce an SV-P image from their offset VSP data.

This paper shows the first-ever example of an SV-P image generated from offset VSP data. An important feature of the SV-P image we show is that the VSP data were generated by a vertical vibrator, not by a horizontal S-wave vibrator. Enhanced upgoing SV-P reflections were extracted from 3-component VSP data using a time-variant receiver rotation approach. Each 3C geophone was steered datapoint-by-datapoint along each VSP trace to the time-varying approach angle of the upgoing SV-P wave. These extracted upgoing SV-P reflections were then imaged using a VSPCDP transformation based on ray-tracing. Comparisons of this SV-P image with its companion P-P and P-SV images show that for deep targets, the image range of SV-P

data is larger than the image range of P-P and P-SV data. Furthermore, the SV-P image is a better description of the Marcellus Shale at our study site than are the corresponding P-P and P-SV images. We also compare the offset VSP SV-P image with a surface-based P-SV seismic profile. These comparisons demonstrate that VSP-based SV-P images can be quite valuable for interpreting near-well geology.

## Description of the far-offset VSP data

The energy source used in this VSP study was a vertical vibrator positioned 4449 ft (1356 m) from the receiver well. The well in which downhole receivers were deployed had a deviation of less than 2-degrees. Receiver stations spanned a depth interval extending from 6570 ft (2003 m) to 220 ft (67 m). The spacing between the receivers was 50 ft (15.2 m).

We show the far-offset VSP data in Figure 1 after the receivers have been rotated by the common procedure of determining a single time-invariant rotation angle for each receiver station. This procedure does a reasonable job of segregating the original data into the downgoing P wavefield and any upgoing events associated with that wavefield (Figure 1a), the downgoing radial-S wavefield SR and any upgoing events associated with that wavefield (Figure 1b), and the downgoing transverse-S wavefield ST and any upgoing events associated with that wavefield (Figure 1c). We see that after these static receiver rotations, upgoing P-P and SV-P wave modes are embedded in the SR wavefield (Figure 1b), and upgoing SV-SV and P-SV wave modes are embedded in the P wavefield (Figure 1a). Any methods for SV-P imaging must separate the upgoing SV-P wavefield from its competing upgoing P-P wave mode. Equally true is that optimal P-SV imaging must concentrate on removing SV-SV reflections that compete with P-SV reflections. Presently, P-SV VSP data processing is done by assuming there are no SV-SV reflections in vertical-vibrator data, which we find to not be a correct assumption. The topic of proper P-SV processing of VSP data will be deferred to a later EGL sponsor report.

Hardage et al. (2014) employed a fixed additional-rotation angle approach to extract upgoing SV-P from far-offset VSP data. This procedure was helpful, but it was not precise because the additional-rotation angle that was applied was a static adjustment, not a dynamic correction. In their work, the difference between the approach angle of upgoing SV-P and P-P wave reflections was fixed at 30 degrees. However, the difference between the approach angles of upgoing SV-P and P-P wave mode varies with both receiver depth and receiver recording time. Therefore, a fixed additional-rotation angle does not result in optimal separation of upgoing SV-P and P-P reflections. In order to get an improved SV-P separation, time-dependent rotation angles should be determined and combined with the depth-dependent difference between the approach angles of upgoing SV-P and upgoing P-P reflections. We calculate these approach-angle differences by ray-tracing.

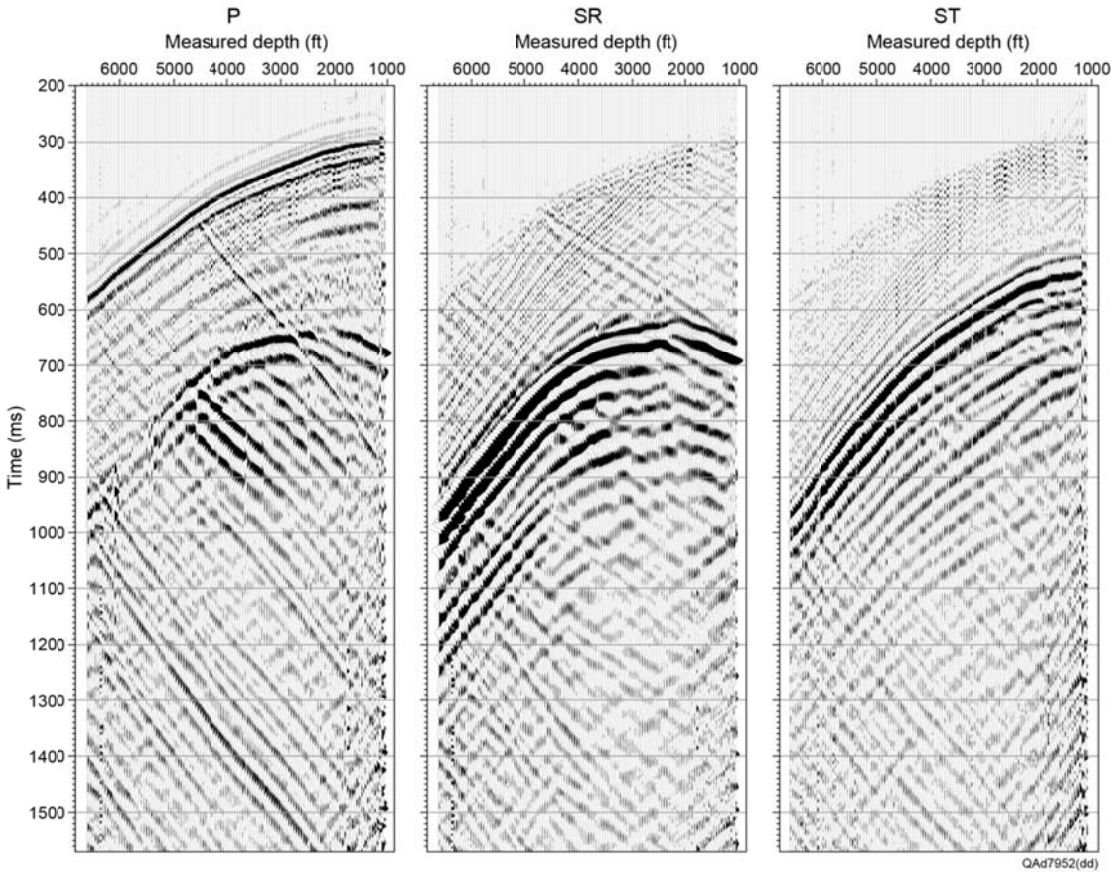


Figure 1. Far-offset VSP data. (a) Downgoing direct-P wavefield and its associated upgoing events. (b) Downgoing radial-S geophone wavefield and its associated upgoing events. (c) Downgoing transverse-S geophone wavefield and its associated upgoing events. The terms radial-S and transverse-S used here refer to the orientations of the geophones that express the data, not to SV and SH wave modes. Data processed by Halliburton.

## Raytracing of offset VSP data

Due to the structural simplicity of our study area, we used a model composed of flat layers of isotropic velocity for ray-tracing. This model considered reflection and refraction of both P and SV modes at all interfaces. The ray-paths were curved as a series of short straight-line segments instead of being a continuous straight line to produce accurate approach angles for P-P and SV-P reflections.

We used zero-offset VSP data to build the isotropic-layer velocity model for the far-offset VSP ray-tracing. The source station in the zero-offset VSP data was only 252 ft (79 m) from the VSP well. The receiver stations were the same for zero-offset and far-offset VSP data. The P-wave and S-wave velocity models we used are shown in Figure 2.

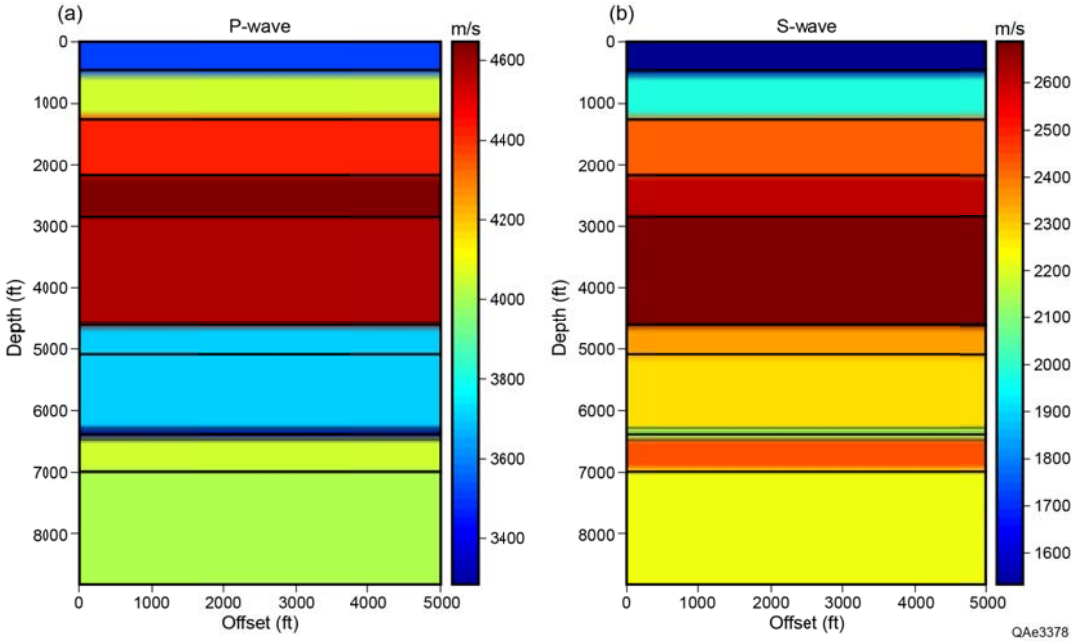


Figure 2. (a) P-wave and (b) S-wave velocity models used in ray-tracing of the far-offset VSP data. The velocities assigned to each layer are isotropic.

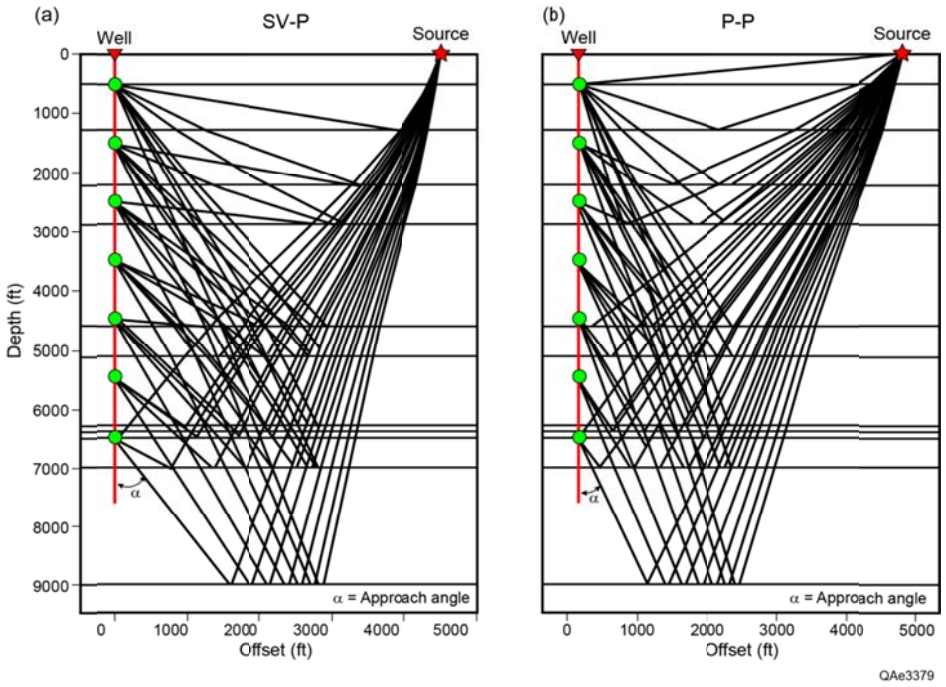


Figure 3. Ray-tracing results for the SV-P (a) and P-P (b) wave modes. The solid red circle marks the position of the source. The green diamonds indicate the positions of receivers. Raypaths from only seven of 128 receivers are plotted to avoid raypath clutter. Angle α is the approach angle for a selected raypath from a single deep interface at a single receiver. Raypaths are straight within each isotropic-velocity layer.

The ray-tracing results for the SV-P and P-P wave modes are shown in Figure 3. For clarity, we show raypaths for only seven receivers of the total 128 receivers. It can be seen from Figure 3 that SV-P raypaths are conspicuously different from P-P raypaths. SV-P reflection points are always closer to the source than to the receiver. The shallower the receiver, the closer SV-P reflection points are to the source. Compared with the raypaths of SV-P and P-P reflections shown in Hardage et al. (2014), the results displayed here are more realistic. Because SV-P and P-P raypaths are different, their respective images differ in position, size, and shape. We will show these differences in the following sections.

We define the approach angle of an upgoing raypath as the angle between the vertical receiver array and the upgoing raypath, as defined by angle $\alpha$ in Figure 3. We see from Figure 3 that the approach angles of upgoing SV-P reflections at a fixed receiver are different for reflections from interfaces at different depths. More important, the differences between the approach angle of upgoing SV-P and P-P reflections at a fixed receiver also differ from each other for reflections from each layer boundary. To better reveal the difference between SV-P and P-P raypaths, we plot both raypaths in a single display (Figure 4). Raypaths are shown for only two receivers, one shallow receiver at a depth of 670 ft (204 m) and a deep receiver at a depth of 5670 ft (1728 m). For shallow receivers, the difference between the approach angles of upgoing SV-P and P-P reflections from shallow interfaces is quite obvious.

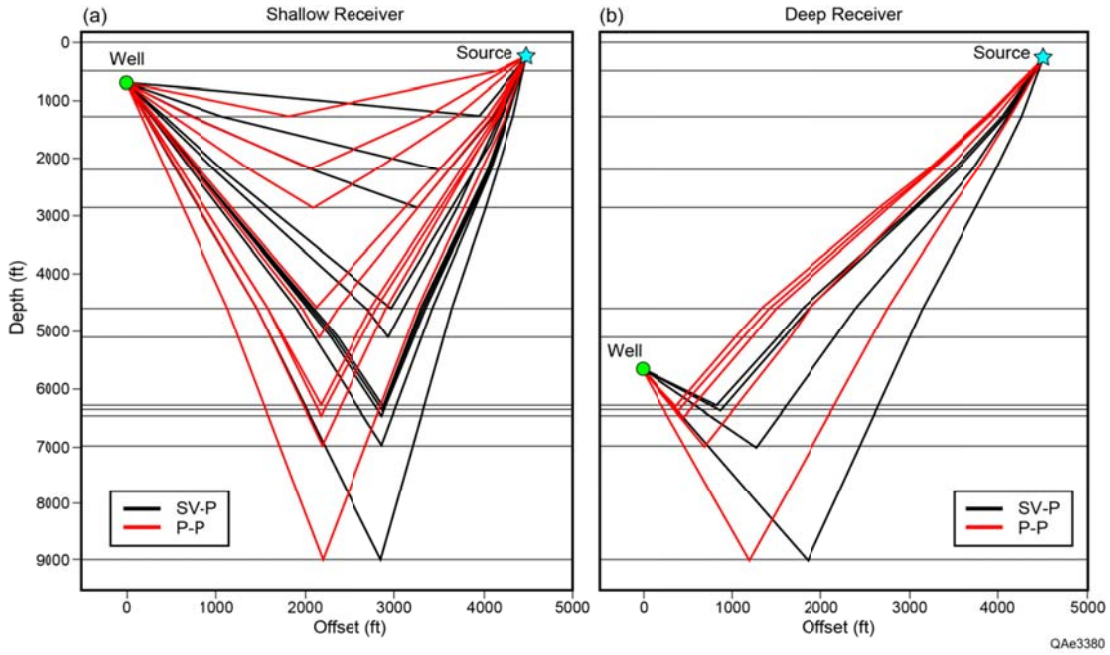


Figure 4. Raypaths of SV-P (black) and P-P (red) wave modes for (a) a shallow receiver at a depth of 670 ft (204 m) and (b) a deep receiver at a depth of 5670 ft (1728 m). The red star marks the position of the source. Green diamonds indicate the positions of receivers.

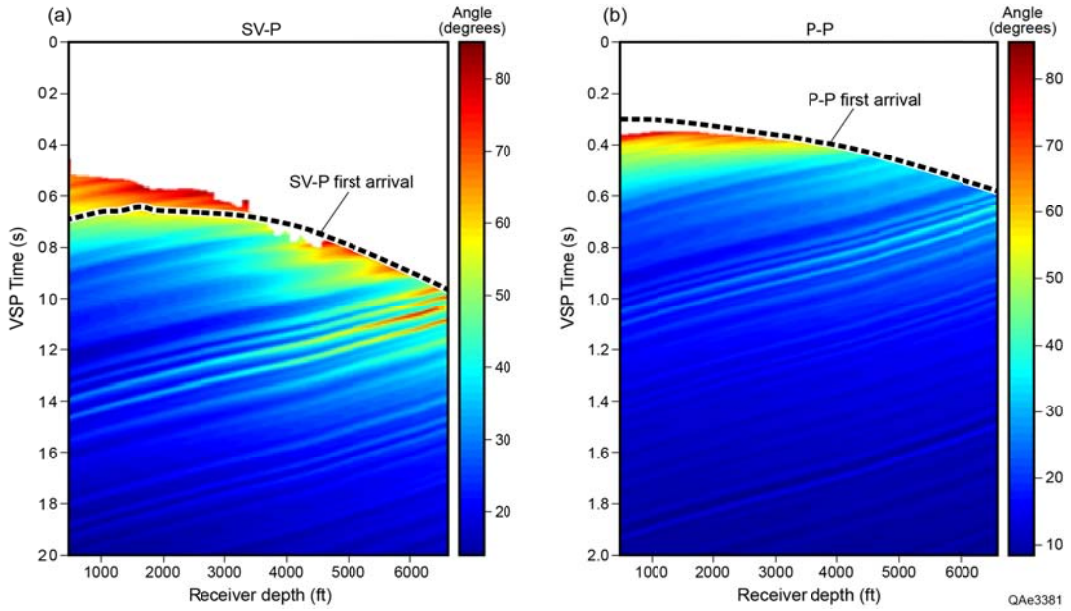


Figure 5. Approach angle (α) of (a) upgoing SV-P reflections and (b) upgoing P-P reflections. The positions of the downgoing SV and P illuminating wavelets are indicated by dashed curves. Approach angles vary not only with receiver depth but also with recording time at each receiver depth.

Because the approach angles of upgoing SV-P and P-P waves vary with the depth of receivers and also with the depth of reflection interfaces, we calculate approach angles of upgoing SV-P and P-P wavefields for all receivers and all reflection interfaces. Figure 5 shows the calculated results. We see that the approach angles of upgoing SV-P raypaths (Figure 5a) and P-P raypaths (Figure 5b) across the two image spaces differ, sometimes significantly. Key concepts are: (1) approach angles at any receiver (a fixed coordinate on the horizontal axis) change with image time (vertical axis), and (2) approach angles at any image time (a fixed point on the vertical axis) change with receiver depth (horizontal axis). Approach angles must be determined in the two-dimensional parameter space of depth and image time shown in Figure 5. This procedure is a departure from the popular VSP data-processing strategy of determining only one approach angle at a receiver station and not varying that receiver rotation as a function of recording time. These differences are large for shallow reflections and are smaller for deep reflections. Thus the separation of upgoing SV-P reflections from upgoing P-P reflections is more difficult for deep layers than for shallow layers.

## Improved SV-P extraction by time-variant rotation

We first show the extracted SV-P wavefield created by a fixed additional-rotation angle approach as employed by Hardage et al. (2014). They incremented the static rotation angle determined for upgoing P-P reflections by an additional rotation angle of 30 degrees to improve the separation of upgoing P-P and SV-P. We display the results in Figure 6 to show the effects of this additional-rotation angle on the separation of upgoing SV-P and upgoing P-P waves.

We see from Figure 6 that this additional rotation step does indeed improve the separation of upgoing SV-P from the competing P-P wave mode. The upgoing P-P reflections with slower apparent velocity are attenuated in Figure 6b and the upgoing SV-P reflections with faster apparent velocity are enhanced. However, there are still some upgoing P-P reflections in the additional-rotation result.

This P-P contamination increases for deeper reflections because the difference between the approach angles of SV-P and P-P reflections is not exactly 30 degrees for reflections from several interfaces. For some interfaces, this angle difference significantly deviates from 30 degrees. We adjust this fixed additional-rotation angle by calculating the differences between the approach angles of upgoing SV-P and P-P reflections for all depth/time coordinates in the VSP data space.

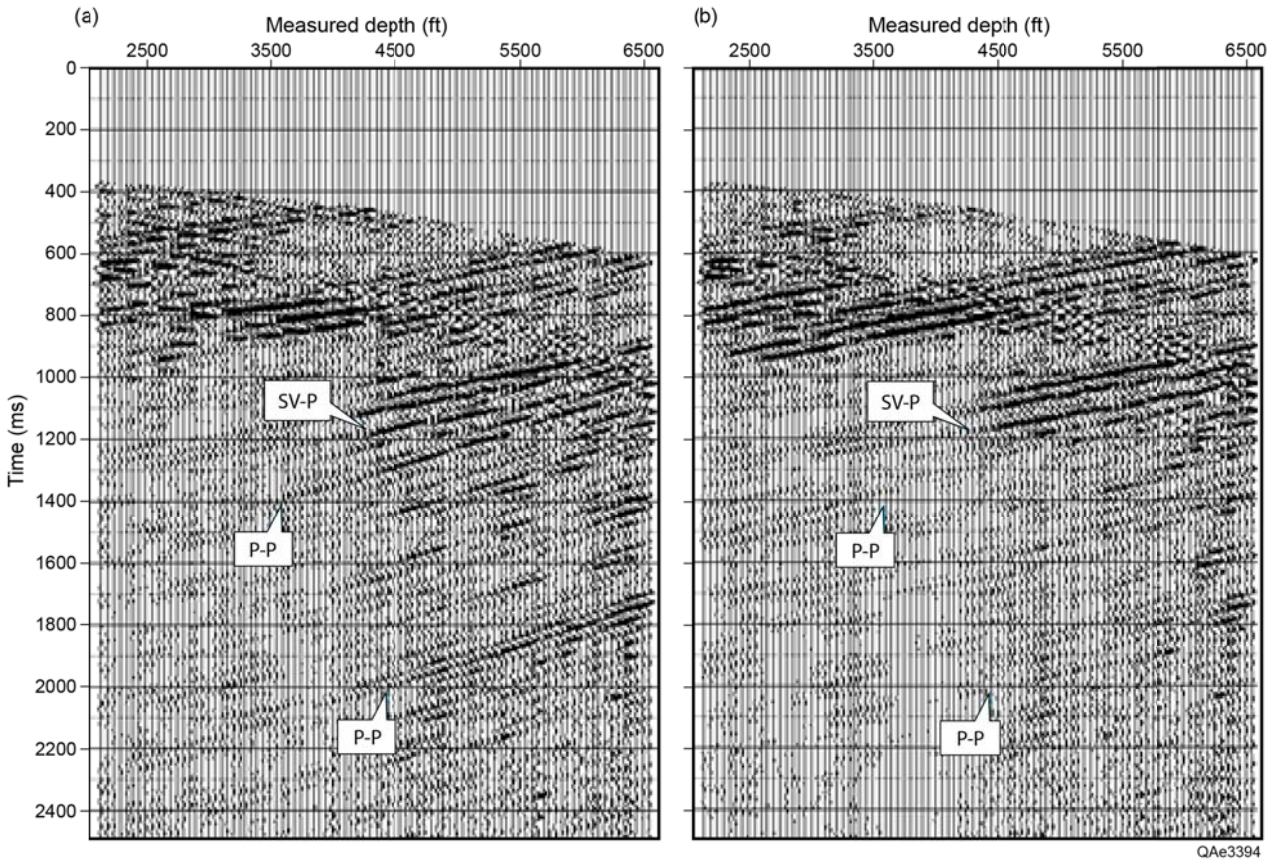


Figure 6. (a) Upgoing VSP wavefield created by using downgoing P direct arrivals as a geophone rotation reference. The resulting wavefield contains both P-P reflections and SV-P reflections. (b) Upgoing VSP wavefield after an additional geophone rotation of 30 degrees in the vertical plane. Note that the upgoing P-P reflections with slower apparent velocity in (a) have been significantly attenuated in (b) after this additional rotation, and upgoing SV-P reflections with faster apparent velocities have been enhanced. Processing by Halliburton.

By dynamically rotating all geophones to the approach angle of the upgoing SV-P wavefield, we were able to obtain an improved separation of upgoing SV-P and P-P reflections. We show the extracted upgoing SV-P data using a fixed additional-rotation approach angle in Figure 7a, and the separated SV-P wavefield using our time-variant rotation angle procedure in Figure 7b. Comparing these results shows that time-variant receiver rotation improves the separation of SV-P reflections from their interfering P-P reflections. The latter extracted upgoing SV-P reflections (Figure 7b) are more continuous and coherent, especially for deep reflections.

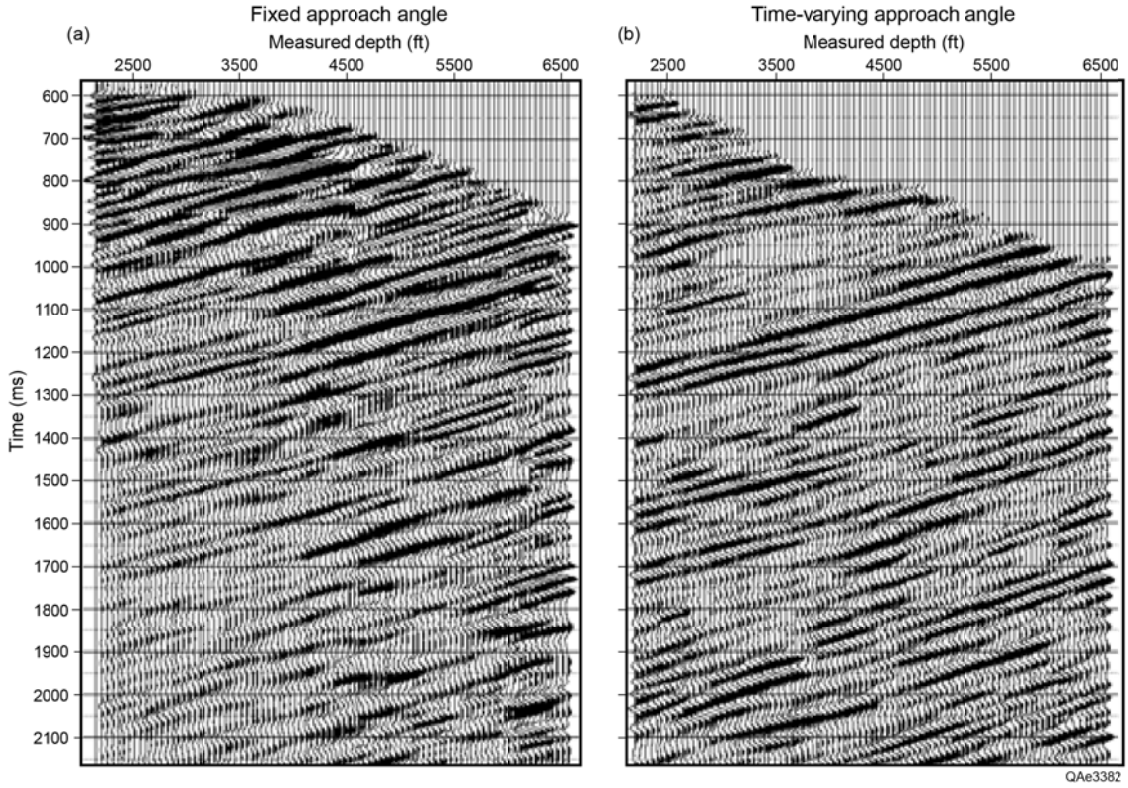


Figure 7. Upgoing SV-P wavefield obtained using (a) a fixed additional-rotation angle of 30 degrees and (b) a time-variant rotation approach. The effects of interfering P-P reflections are reduced in option (b).

## Imaging of SV-P by VSPCDP transform

We use the VSPCDP transformation described by Hardage (2000) to produce an image from the upgoing SV-P reflections. This procedure is based on the ray-tracing concepts discussed in the previous section, which generate reflection-point coordinates and zero-offset, two-way vertical traveltimes of reflection events at each receiver. The results are shown in Figure 8. We also show the images of the upgoing P-P and P-SV reflections derived from the same far-offset VSP data.

In Figure 8, offset is measured from the receiver well. Comparison of the SV-P, P-P, and P-SV images shows that the SV-P image enhances the imaging of deep layers. The image offset range of SV-P data for deep formations like the Marcellus Shale at our study site is wider than the image widths of the companion P-P and P-SV wave modes. The P-SV image of the Marcellus Shale is distorted by the competing SV-SV wave mode embedded in the same receiver response. Specifically, SV-SV reflections from the shallower Tully (Figure 8) are interfering with the Marcellus P-SV reflections. This interference is based on the following relationship between SV-SV and P-SV image-time coordinates from a target interface:

$$T_{SS} = 2T_{PS} / [1 + (V_S/V_P)].$$

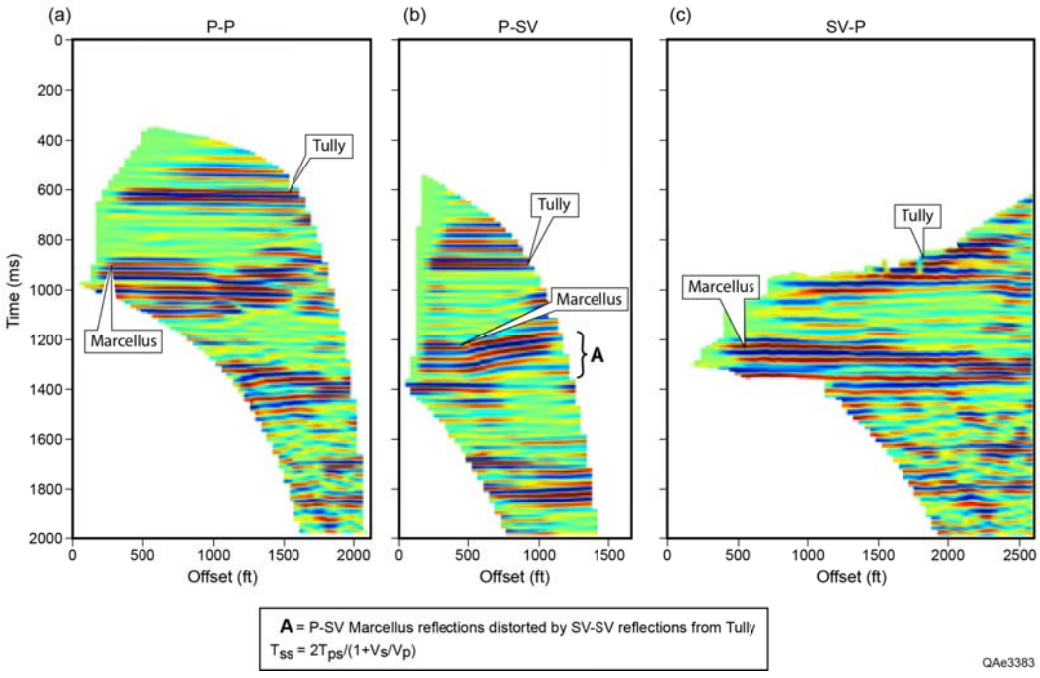


Figure 8. VSPCDP transformation of (a) upgoing P-P, (b) upgoing P-SV, and (c) upgoing SV-P reflections in the time domain. The offset image range of the SV-P wave for deep formations like the Marcellus Shale (c) is wider than the offset dimensions of its companion P-P and P-SV wave modes (a and b). The P-SV image of the Marcellus Shale (b) is affected by interfering SV-SV reflections. Improved procedures for creating P-SV images will be discussed in a subsequent paper that is being prepared.

In this equation, $T_{SS}$ is the image time of SV-SV data, $T_{PS}$ is the image time of P-SV data, and $V_S/V_P$ is the ratio of S velocity to P velocity. Referring to Figure 8b, the Tully P-SV reflection occurs at approximately 900 ms. The average $V_P/V_S$ ratio is approximately 1.8, so $V_S/V_P = 0.55$. These parameters cause the Tully SV-SV reflection to occur at an image time of $T_{SS} = 1160$ ms. These interfering Tully SV-SV reflections cause the Marcellus P-SV reflections to be incorrectly uplifted to 1160 ms at mid-to-far offsets (Figure 8b).

Common VSP data-processing procedures ignore the possibility that SV-SV reflections exist in VSP data generated by a P-wave source. However, research done at the Exploration Geophysics Laboratory shows robust SV-SV reflections can be produced by P-wave sources. We are initiating a companion paper that will illustrate how dynamic VSP receiver rotation prevents SV-SV reflections from being in P-SV data and improves the quality of P-SV images.

One of the advantages of VSP data is that they provide a rigorous relationship between time and depth. Therefore, we can easily convert the SV-P, P-P and P-SV images in Figure 8 from the time domain to the depth domain. The results are shown in Figure 9. The differences in SV-P, P-P, and P-SV images are also obvious in these depth-domain views. These images show that at this location, SV-P data provide a larger and better-quality image of the Marcellus Shale and other deep geology than do P-P and P-SV data. One feature of SV-P images that will be a new concept for interpreters is that an SV-P image never "touches" the receiver well as do P-P and P-SV images. The inability of an SV-P image to touch a receiver well is caused by Snell's Law that forces SV-to-P reflection points to always be closer to the source than to the receiver.

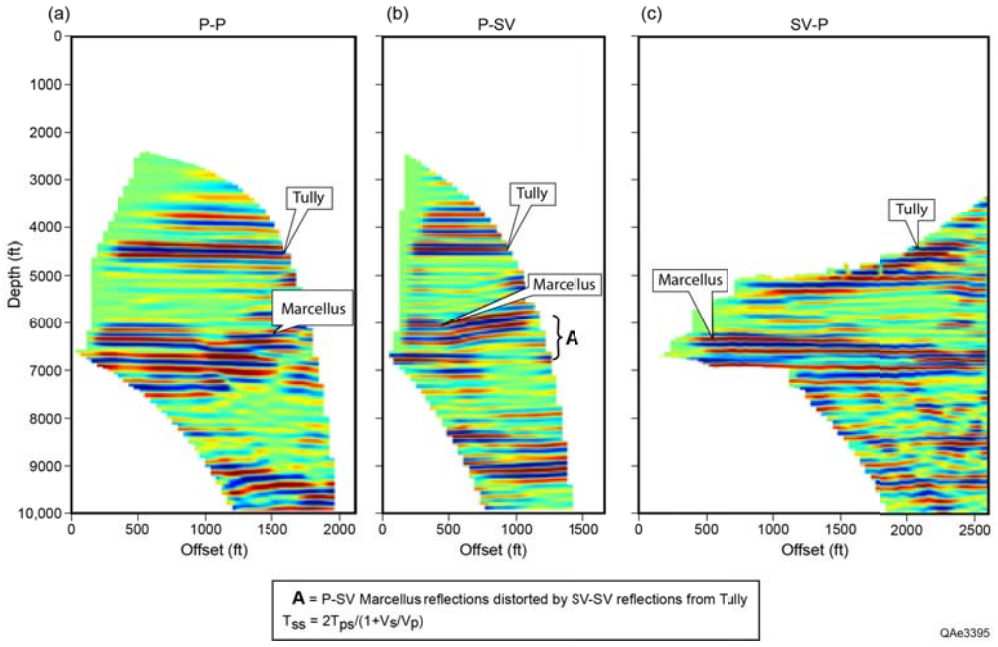


Figure 9. VSPCDP transformation of (a) upgoing P-P, (b) upgoing P-SV and (c) upgoing SV-P reflections in the depth domain. The offset image range of the SV-P wave (c) is wider than the offset dimensions of the P-P and P-SV waves (a and b) for deep formations like the Marcellus Shale. The SV-P image also exhibits an enhanced characterization of the Marcellus Shale compared to the P-P and P-SV images.

## Comparison of VSP image with surface seismic data

A 3C3D seismic data volume was recorded around the well where the VSP data were acquired. The energy sources used in this 3D seismic program were shot-hole explosives positioned at a depth of 6 m. Buried explosives are another type of vertical-force source like the vertical vibrator that generated the VSP data. Figure 10 shows a P-P profile passing through the receiver well and the VSP source station. The corresponding P-P image of the far-offset VSP data is shown in Figure 10 for comparison.

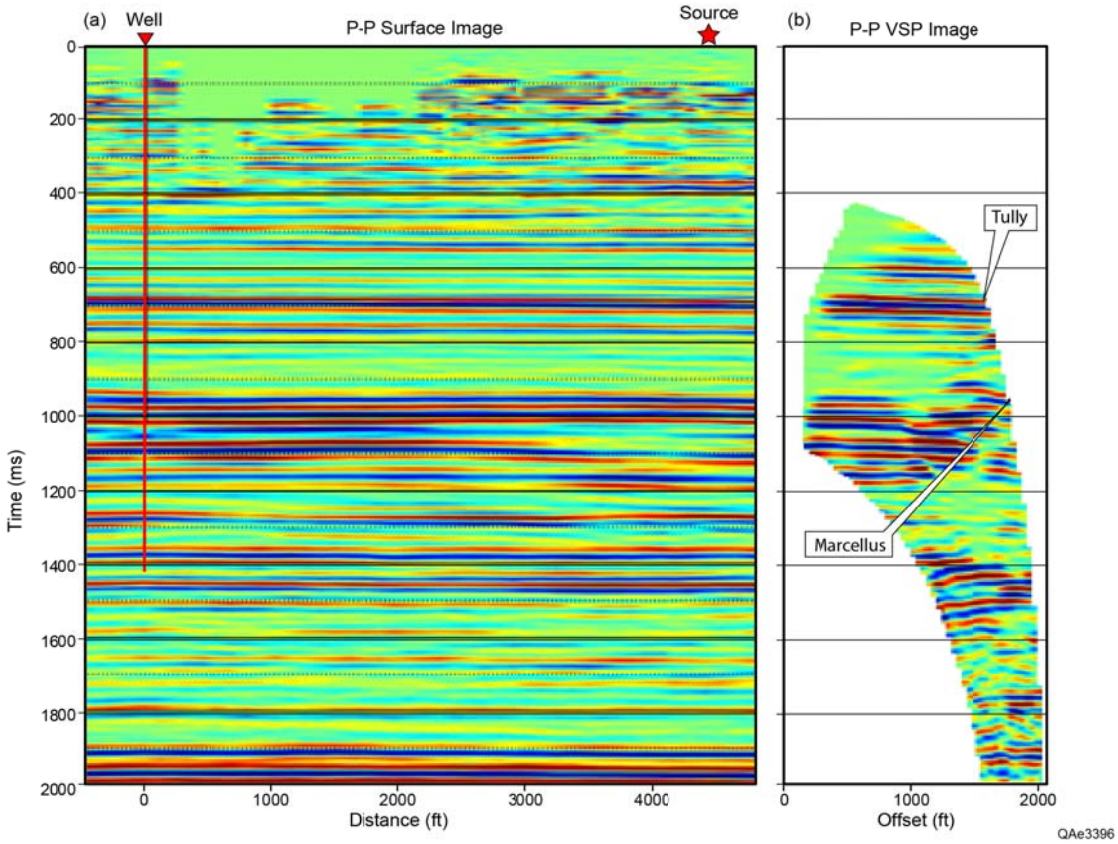


Figure 10. Comparison of (a) P-P surface-based seismic profile intersecting the VSP well (marked by red triangle) and the VSP source station (marked by red star) and (b) P-P image from the far-offset VSP data.

We show the far-offset VSP SV-P image and the surface-based P-SV image along the same profile in Figure 11. We have not yet completed our processing of surface-based SV-P seismic data so that a surface-based SV-P profile can be shown for comparison. However, surface-based P-SV and SV-P data should create equivalent images so the use of this P-SV profile will be sufficient to illustrate the validity of our SV-P VSP image. The equivalence between P-SV and SV-P imaging is perhaps better seen when the VSP-based SV-P image is superimposed on the surface-based P-SV image as shown in Figure 12. Comparing Figures 10 through 12, we found SV-P images made from VSP data are better for analyzing large-offset variations of geologic targets local to a VSP well than are either P-P or P-SV images constructed from the same VSP data. Therefore, the extraction and imaging of SV-P reflections can be of great importance for seismic interpreters.

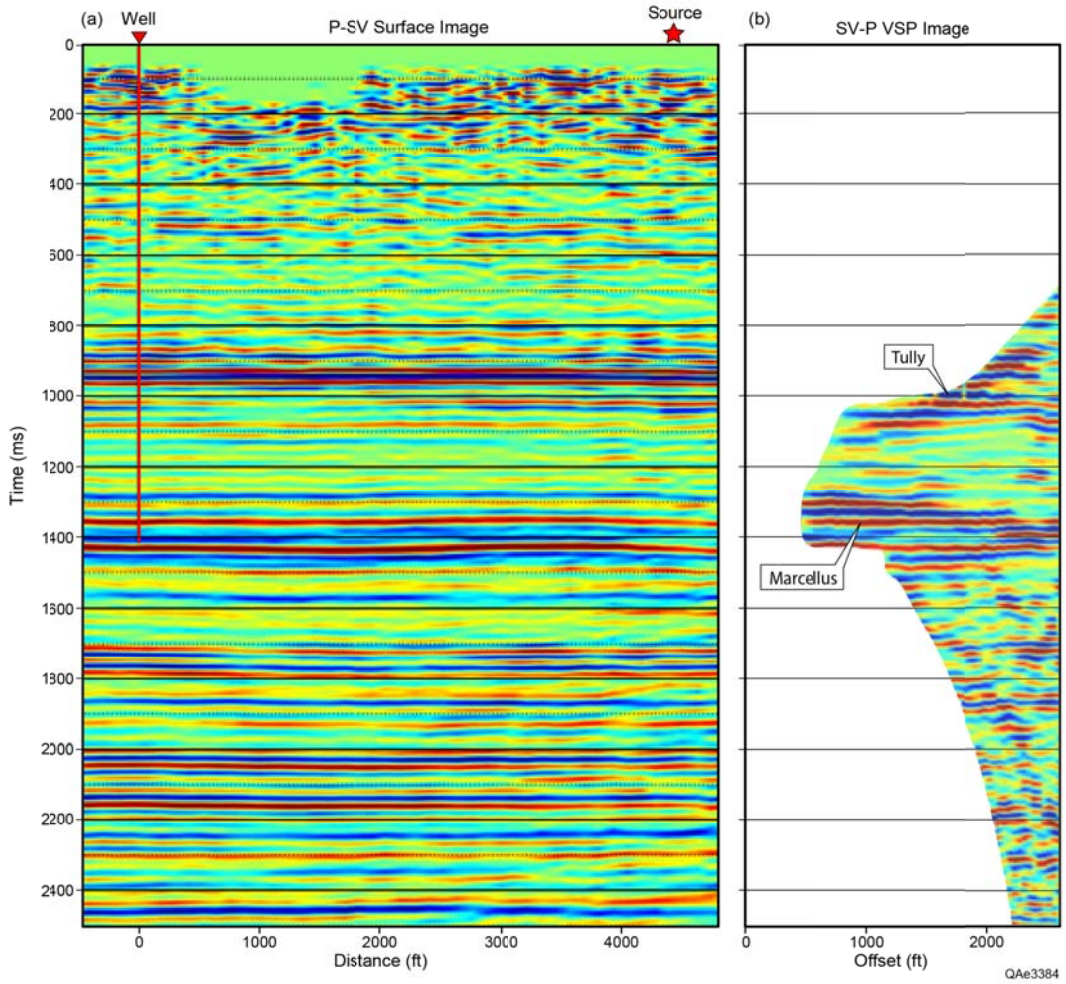


Figure 11. Comparison of (a) surface-based P-SV seismic profile with (b) the SV-P image from the far-offset VSP data.

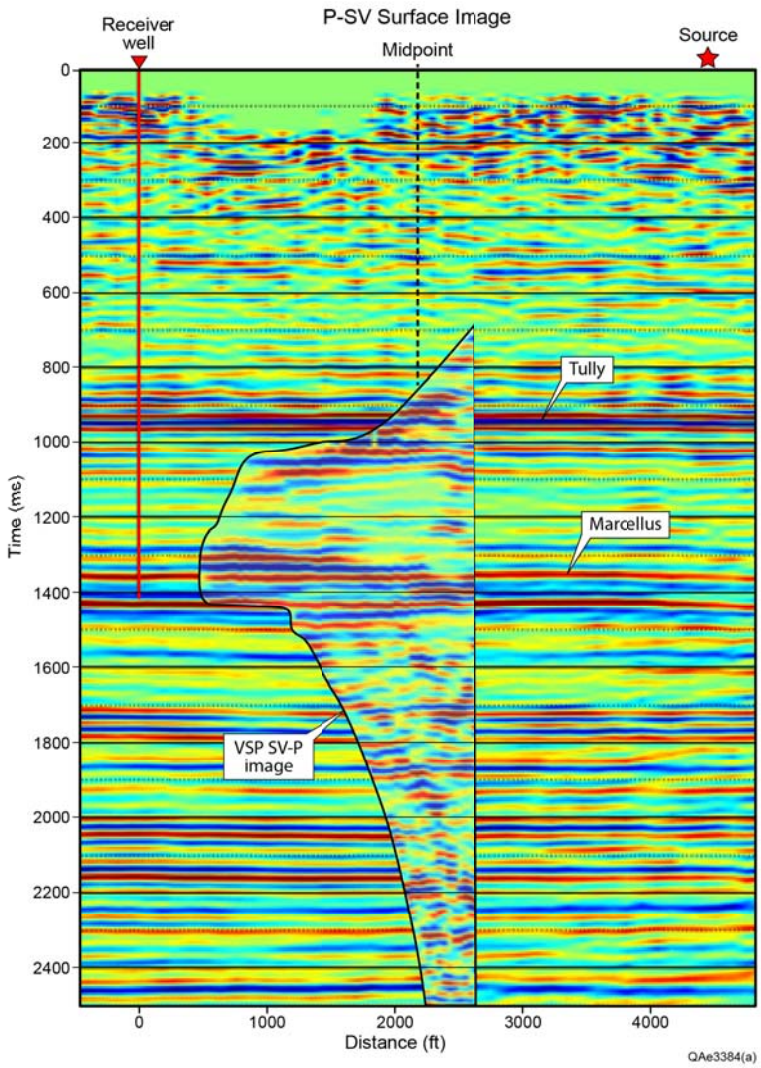


Figure 12. A variation of Figure 11 in which the SV-P image is superimposed on the P-SV profile.

## Discussion and Conclusions

The SV-P mode is a valuable wave embedded in vertical-geophone P-wave data. However, the SV-P wave-mode has long been ignored by the geophysical industry. This report demonstrates that upgoing SV-P reflections can be extracted from far-offset VSP data generated by a vertical vibrator source. To our knowledge, the SV-P image shown in this paper is the first SV-P image that has ever been made from VSP data. This SV-P image is especially unique because the illuminating SV wavefield was produced by a vertical-displacement source (a vertical vibrator in this case) and not by a horizontal vibrator.

The match between the P-SV and SV-P images in their respective image-time domains confirms that the illuminating SV wavefield that produced the SV-P data was generated directly at the vertical-vibrator source station just as was the illuminating P wavefield that produced the P-SV data. If the illuminating SV wavefield was produced at an interface below the vertical vibrator by P-to-SV mode conversion, the P-SV and SV-P images would not have identical image-time coordinates. This fundamental wave propagation physics - that vertical-displacement sources produce S-wave modes directly at the source station just as they do direct-P modes - has been documented with real seismic data and field experiments by Hardage and Wagner (2014).

VSP SV-P images have interesting features: (1) they extend across a wider offset range than do P-P and P-SV images, (2) they extend farther from the receiver well than do P-P and P-SV images, and (3) they never touch the receiver well as do P-P and P-SV images. This new SV-P option for imaging geology can have great significance for seismic interpreters. Regarding points 1 and 2, an interesting observation is that some VSP data processors have noted that P-P VSP images can be extended to greater offsets from a receiver well if P-P multiples are included in the imaging process. We now wonder if what these processors considered to be P-P multiple reflections were actually converted SV-P reflections.

The ray-tracing model used in this paper was a stack of horizontal, isotropic-velocity layers. Our assumption of horizontal isotropic layering works reasonably well for the far-offset VSP data used in this paper because of the relatively simple geological structure local to the receiver well and the mild anisotropy of the seismic propagation medium. More complex velocity models which allow lateral velocity variations and anisotropic velocities will be needed to improve our ray-tracing at some locations. The need for more complex velocity models is needed even at our study site for shallow layers where some anisotropy is apparent.

Our next objective is to compare SV-P images derived from VSP data with SV-P images recorded with surface-based receivers. For all users of VSP technology, we must emphasize that a rich amount of S-wave information exists in legacy VSP data that have been acquired with P-wave sources for the past two or three decades. These legacy VSP data provide a low-cost option for creating S-wave information and studying S-wave applications by using the SV-P and S-S modes that are embedded in the data by P-wave sources.

## Acknowledgments

We thank Chesapeake Energy for providing access to the VSP data we used. Geokinetics and Geophysical Pursuit provided the 3C3D seismic data. The lead author, Yandong Li, was a visiting scientist at the Exploration Geophysics Laboratory for six months and appreciates The University of Texas at Austin for providing the opportunity to do this VSP study. The work is partially-supported by the State Key Science and Technology Project on Marine Carbonate Reservoir Characterization, China (2011ZX05004-003).

## References

DeAngelo, M. V., and B. A. Hardage, 2014, Application of 3C/3D converted mode reflections, King County, Texas: Interpretation, **2**, No.3, SE39-SE45.

Fraiser, C., and D. Winterstein, 1990, Analysis of conventional and converted mode reflections at Putah sink, California using three-component data: Geophysics, **55**, 646-659.

Guy, E. D., 2004, Evaluation of near-surface converted mode seismic reflection imaging potentials: Electronic Journal of Geotechnical Engineering, **9**, 1-35.

Hardage, B. A., 2000, Vertical seismic profiling, Part A, principles, 3rd updated and revised ed: Pergamon.

Hardage, B. A., D. Sava, D. Wagner, 2014, SV-P: an ignored seismic mode that has great value for interpreters: Interpretation, **2**, No. 2, SE17-SE27, httdoi.org/10.1190/INT-2013-0096.1.

Hardage, B.A., and D. Wagner, 2014, Generating direct-S modes with simple, low-cost, widely available seismic sources: Interpretation, **2**, No. 2, SE1-SE16, doi10.1190/INT-2013-0095.1.